

# 1 Hygrothermal properties of compressed earthen bricks

2 Lei Zhang <sup>a</sup>, Liu Yang <sup>a,b,\*</sup>, Bjørn Petter Jelle <sup>c,d</sup>, Yu Wang <sup>e</sup>, Arild Gustavsen <sup>f</sup>

3 <sup>a</sup> *College of Architecture, Xi'an University of Architecture and Technology, Shaanxi 710055, China*

4 <sup>b</sup> *State Key Laboratory of Green Building in West China, Xi'an, Shaanxi 710055, China*

5 <sup>c</sup> *Department of Materials and Structures, SINTEF Building and Infrastructure, Trondheim, Norway*

6 <sup>d</sup> *Department of Civil and Environmental Engineering, Norwegian University of Science and Technology (NTNU), Trondheim,*  
7 *Norway*

8 <sup>e</sup> *Department of Architecture and Planning, Norwegian University of Science and Technology (NTNU), Trondheim, Norway*

9 <sup>f</sup> *Department of Architecture and Technology, Norwegian University of Science and Technology (NTNU), Trondheim, Norway*

## 10 Abstract

11 The present study investigates the relationship between bulk density and hygrothermal behaviour of  
12 compressed earthen bricks. The experimental results show that the thermal conductivity linearly  
13 increases from 0.5228 W/(m K) to 0.9308 W/(m K) as the bulk density increases, and that the equilibrium  
14 moisture content increases with increasing relative humidity. Hysteresis effects are observed. When  
15 relative humidity changes, compressed earthen bricks usually reach an equilibrium in four days and it  
16 means compressed earthen bricks can be used to regulate indoor relative humidity. The hysteresis values  
17 of compressed earthen bricks with different bulk densities are close to each other, especially low relative  
18 humidity, as the results of Brunauer-Emmett-Teller (BET) show that samples with different bulk densities  
19 have similar porous structure including specific surface area (15.5008 ~ 16.2091 m<sup>2</sup>/g), micropore  
20 volume (0.000867 ~ 0.001221 cm<sup>3</sup>/g) and mesopore volume (0.030785 ~ 0.032239 cm<sup>3</sup>/g). Moreover,  
21 the hysteresis loops in this study belong to the type H3 hysteresis loops which indicate that there are  
22 some slitlike pores inside the matrix.

## 23 Keywords

24 Hygrothermal properties; Thermal conductivity; Hygroscopic behaviour; Porous structure; Compressed

---

\* Corresponding author.

E-mail address: yangliu@xauat.edu.cn (L. Yang).

25 earthen brick.

26 Highlights:

- 27 ● Thermal conductivity of compressed earthen bricks increases with increasing bulk density.
- 28 ● The response of compressed earthen bricks to a relative humidity change is rather fast.
- 29 ● Hysteresis values of compressed earthen bricks increased with increasing relative humidity.
- 30 ● Hygroscopic properties of compressed earthen bricks with different bulk densities are close to
- 31 each other.

## 32 1. Introduction

33 The increased use of non-renewable resources and increased greenhouse gas emissions result in  
34 growing environmental problems. The impact of building performance on the ecological environment  
35 gradually attracts more and more public attention. In the western world, buildings account for  
36 approximately a third of both all energy use and greenhouse gas emissions [1]. In China, energy  
37 consumption in commercial and residential buildings has considerably increased in recent years, the  
38 building energy demand will account for 35 % of the total energy consumption in 2020 [2]. The energy  
39 requirement for heating, cooling and ventilation accounts for the major part of the building energy  
40 consumption. Therefore, several solutions have been implemented to reduce energy consumption, e.g.  
41 promotion of increased levels of thermal insulation, use of renewable energy and promotion of energy  
42 efficiency [3,4]. Besides, the application of the environmental friendly building materials will be  
43 important to reduce embodied emissions (i.e. emission related to building material production and  
44 maintenance) [4]. Earth-based materials may be important in this respect [5,6]. They can also have  
45 hygrothermal properties that can result in a more stable indoor environment [7].

46 The hygrothermal properties of building materials can influence the ability of indoor climate  
47 stabilization of buildings. For example, a well-insulated building envelope can reduce the heat transfer  
48 through the building envelope and weaken the impact of outdoor climate changes on indoor environment.  
49 Materials with good moisture storage abilities, on the other hand, are able to absorb water vapour from

50 the air when the relative humidity increases and release water vapour when the relative humidity  
51 decreases in order to maintaining a more stable indoor relative humidity [7,8]. In situations where a more  
52 stable indoor relative humidity is desirable, the building envelope should have the ability of moisture  
53 storage.

54 Soil and/or earthen materials have been used for construction purpose for thousands years; and  
55 nowadays, approximately one half of the world's population still live in earthen buildings [7,9].  
56 Compared with some common building envelope materials, i.e. fired clay bricks and concrete, earthen  
57 materials have a larger moisture capacity [10]. This can be explained from that earthen materials are  
58 typical porous materials that have a moisture storage capability caused by single layer adsorption, multi-  
59 layer adsorption and capillary condensation [11]. More importantly, as a natural, sustainable and eco-  
60 friendly building material, the abundant source of earthen materials can lead to direct site-to-service  
61 application, thus reducing the costs caused by acquisition, transportation and production.

62 During the last few years, a growing interest has appeared for the hygrothermal properties of earthen  
63 materials. Liuzzi et al. [9] and Cagnon et al. [12], respectively, conducted experimental studies to  
64 compare the thermal conductivity values between earthen bricks from different regions; the results  
65 showed that the differences of mineral composition and grading level have a huge impact on the thermal  
66 conductivity values of earthen bricks. Hall et al. [13], Mansour et al. [14] and Tang et al. [15] studied the  
67 effect of bulk density, water content and degree of saturation on the thermal conductivity of compressed  
68 earthen bricks. Results demonstrated that there is a linear correlation between the thermal conductivity  
69 and density and then the thermal conductivity significantly increases with increasing degree of saturation.  
70 Taallah et al. [16], Ashour et al. [17] and Adam et al. [18] respectively added natural fibers and chemical  
71 additives into earthen materials to produce stabilized earthen materials, where the results demonstrated

72 that natural fibers are able to reduce the thermal conductivity as the fibres contain a lot of pores.  
73 Conversely, cementitious products formed by hydration reaction increase the thermal conductivity of  
74 stabilized earthen materials. For hygroscopic behaviour of earthen bricks, Liuzzi et al. [9] and Cagnon  
75 et al. [12] measured earthen bricks from different regions and results indicated that there are obvious  
76 differences between them as mineral composition of earthen materials has a serious influence on the  
77 adsorption and desorption ability. Ashour et al. [19,20] presented that addition of natural fibers increases  
78 the equilibrium moisture content of earthen materials; however, cementitious materials, i.e. cement, lime  
79 and gypsum, have the opposite effect on the equilibrium moisture content [11,20]. McGregor et al. [21]  
80 indicated that the variation of density influences the pore structure and therefore affects the capillary  
81 condensation which leads to the significant increase of the equilibrium moisture content. Raimondo et  
82 al. [22] and Randazzo et al. [23] measured the pore size and specific surface area of earthen materials by  
83 helium pycnometry and Brunauer-Emmett-Teller (BET) method and obtained the correlation between  
84 the porous structure and hygroscopic behaviour.

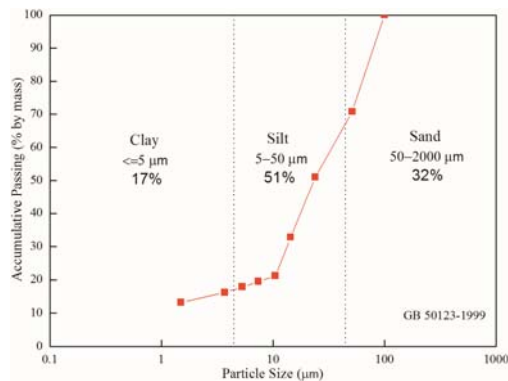
85 It is noteworthy that the presented studies have essentially considered the thermal properties or  
86 hygroscopic properties of earthen materials, and very few papers have investigated the hygrothermal  
87 properties of earthen materials and, in particular, compressed earthen bricks. The objective of this study  
88 is to investigate how the porous structures of compressed earthen bricks vary with change of bulk density  
89 and then the effect of the porous structure on the hygrothermal properties of compressed earthen bricks.  
90 Additionally, such studies presented that bulk density has a significant effect on thermal or hygroscopic  
91 properties of earthen materials and that bulk density is a rural macroscopic physical indicator which is  
92 easier to control in the production process of earthen bricks. Furthermore, the aim of this study is to try  
93 to obtain a relationship between hygrothermal properties and bulk density in order to guide the

94 preparation of compressed earthen bricks to reach the requirements concerning hygrothermal behavior.

## 95 2. Experimental

### 96 2.1. Materials

97 The earthen materials used in this investigation derive from Turpan, located at 42°26' N, 89°5' W in  
98 the Xinjiang Uygur Autonomous Region, Northwest of China. The grading curves and the particle sizes  
99 of the earthen materials were investigated by grain size analysis, according to GB/T 50123-1999 [24].  
100 The composition of the earthen material is 17 % clay (less than 5  $\mu\text{m}$ ), 51 % silt (between 5 and 50  $\mu\text{m}$ )  
101 and 32 % sand (between 50 and 2000  $\mu\text{m}$ ). The test results are presented in Fig. 1.

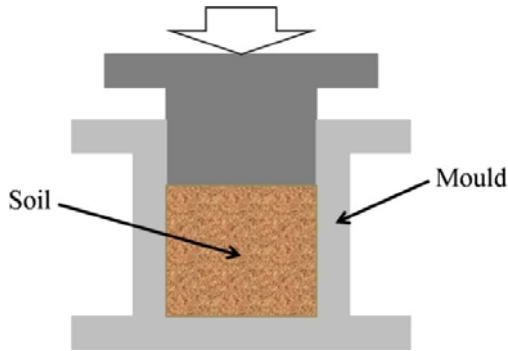


102  
103 Fig. 1 Grain size distribution of earthen material used.

### 104 2.2. Sample preparation

105 Before the preparation of compressed earthen samples, the earthen material was sieved to remove the  
106 oversized gravel (larger than 2 mm diameter) and organic matter. The sieved material was dried in air at  
107 a temperature of 105  $^{\circ}\text{C}$  to obtain a constant weight. To produce the compressed earthen samples at  
108 different bulk densities, the dried material put into the mould was controlled and the mass of dried  
109 material inside the mould was determined by the calculation of target bulk density times volume of mould.

110 The classification of bulk density includes 1.5, 1.7, 1.9 and 2.1 g/cm<sup>3</sup> and the sample dimensions were  
111 50 mm × 50 mm × 25 mm. Samples were prepared by a hydraulic press under a pressure of from 20 to  
112 70 kN, as shown in Fig. 2. After compaction, the samples were placed in controlled laboratory conditions  
113 for 14 days to avoid cracking. The environmental temperature and relative humidity in the laboratory  
114 during the drying process were 20 °C and 60 %, respectively.



115

116 Fig. 2 Process of compaction of samples.

## 117 2.3. Characterization

### 118 2.3.1. Physical and chemical characterization

119 The earthen material was characterized by some basic tests including Atterberg limit and chemical  
120 composition. The Atterberg limits were determined by the Liquid-plastic Tester according to JTJ051-93  
121 [25] and results are shown in Table 1. The plastic index is 5.5 % which means the earthen material  
122 belongs to silty clays and is suitable for production of compressed earthen bricks [26]. The chemical  
123 composition of the earthen material was estimated on the basis of x-ray fluorescence and results are given  
124 in Table 2. The earthen material in this study was mainly composed of silica, calcium oxide and alumina.  
125 Taking into account the above results, it could be concluded that the earthen material was rich in quartz,  
126 calcite and aluminum minerals.

127 Table 1 Atterberg limits of the earthen material.

| Atterberg limits |        |
|------------------|--------|
| Liquid limit     | 23.7 % |
| Plastic limit    | 18.2 % |
| Plasticity index | 5.5 %  |

128 Table 2 Chemical composition of soil used (wt%).

| SiO <sub>2</sub> | Al <sub>2</sub> O <sub>3</sub> | Fe <sub>2</sub> O <sub>3</sub> | CaO    | MgO   | Na <sub>2</sub> O | K <sub>2</sub> O | SO <sub>3</sub> | TiO <sub>2</sub> | MnO   | ZrO <sub>2</sub> |
|------------------|--------------------------------|--------------------------------|--------|-------|-------------------|------------------|-----------------|------------------|-------|------------------|
| 47.770           | 12.210                         | 8.845                          | 19.367 | 4.261 | 3.980             | 1.940            | 0.454           | 0.860            | 0.231 | 0.082            |

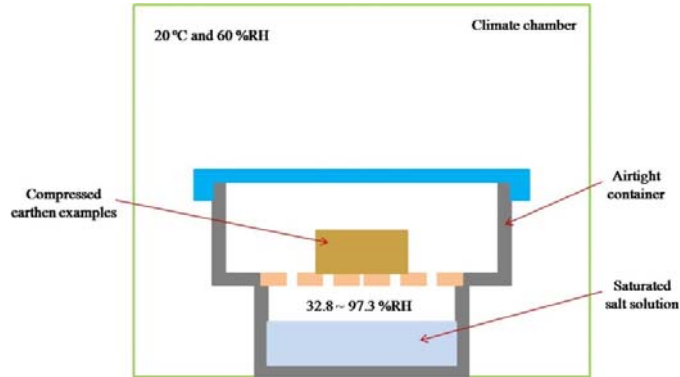
129 2.3.2. Adsorption-desorption isotherms

130 Adsorption-desorption isotherms are comprised of an adsorption branch which indicates the tested  
 131 specimen adsorbs water vapour from the surrounding at a series of relative humidity and a desorption  
 132 branch which presents the tested specimen releases water vapour to surrounding to reach an equilibrium.  
 133 In this study, method of saturated salt solutions was used to measure adsorption-desorption isotherms of  
 134 compressed earthen samples in order to describe the hygroscopic behaviour according to GB/T 20312-  
 135 2006 [27]. All samples were previously oven dried at 105 °C to reach a constant mass. Six relative  
 136 humidities, i.e.  $32.8 \pm 0.2$ ,  $43.2 \pm 0.1$ ,  $52.9 \pm 0.2$ ,  $64.9 \pm 0.2$ ,  $84.3 \pm 0.1$  and  $97.3 \pm 0.3$  % RH, were used  
 137 for tests and different relative humidity were obtained using saturated salt solutions (Table 3). The dried  
 138 samples were placed on the plastic meshes over airtight containers which were contained with various  
 139 saturated salt solutions from low to high, respectively (Fig. 3). The airtight containers were placed inside  
 140 a chamber at 20 °C and 60 % RH and then the samples were weighed periodically until the variation of  
 141 two consecutive results 24 h apart was less than 0.1 %. When the tested samples reached a moisture  
 142 equilibrium at  $97.3 \pm 0.3$  % RH condition, the adsorption branch tests were finished and samples were  
 143 transferred immediately into the  $84.3 \pm 0.1$  % RH condition to measure the desorption branch. The tested  
 144 samples were placed in the lower relative humidity after reaching an equilibrium at a certain relative

145 humidity. The desorption branch tests were completed when the tested examples reached an equilibrium  
 146 at  $32.8 \pm 0.2$  % RH condition.

147 Table 3 Saturated salt solutions used for obtaining different relative humidity.

| Molecular formula | MgCl <sub>2</sub> | K <sub>2</sub> CO <sub>3</sub> | Mg(NO <sub>3</sub> ) <sub>2</sub> | CoCl <sub>2</sub> | KCl        | K <sub>2</sub> SO <sub>4</sub> |
|-------------------|-------------------|--------------------------------|-----------------------------------|-------------------|------------|--------------------------------|
| Relative humidity | 32.8±0.2 %        | 43.2±0.1 %                     | 52.9±0.2 %                        | 64.9±0.2 %        | 84.3±0.1 % | 97.3±0.3 %                     |
|                   | RH                | RH                             | RH                                | RH                | RH         | RH                             |

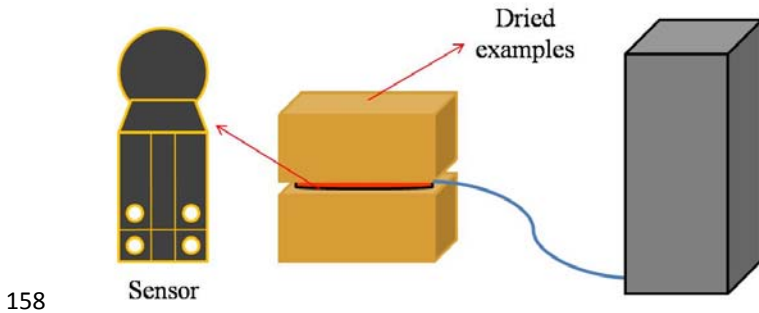


148  
 149 Fig. 3 Operation conditions for adsorption-desorption isotherms.

150 2.3.3 Thermal conductivity

151 The thermal conductivity values of compressed earthen samples were measured by using a Hot Disk  
 152 apparatus (TPS-2500 S) according to ISO/DIS 22007-2:2015 [28]. Prior to testing, the equipment was  
 153 calibrated with an expanded polystyrene board to ensure the accuracy of the tested results and the flatness  
 154 of samples was checked to make a perfect contact between the sensor and the surface of sample, as shown  
 155 in Fig. 4. Additionally, the samples were oven dried at 105 °C for 24 hours in order to measure the dry  
 156 thermal conductivity of the samples .Each measurement was repeated three times and the mean value  
 157 was reported.





158  
159 Fig. 4 Experimental setup for thermal conductivity measurements by using Hot Disk apparatus.

#### 160 2.3.4 Pore structure

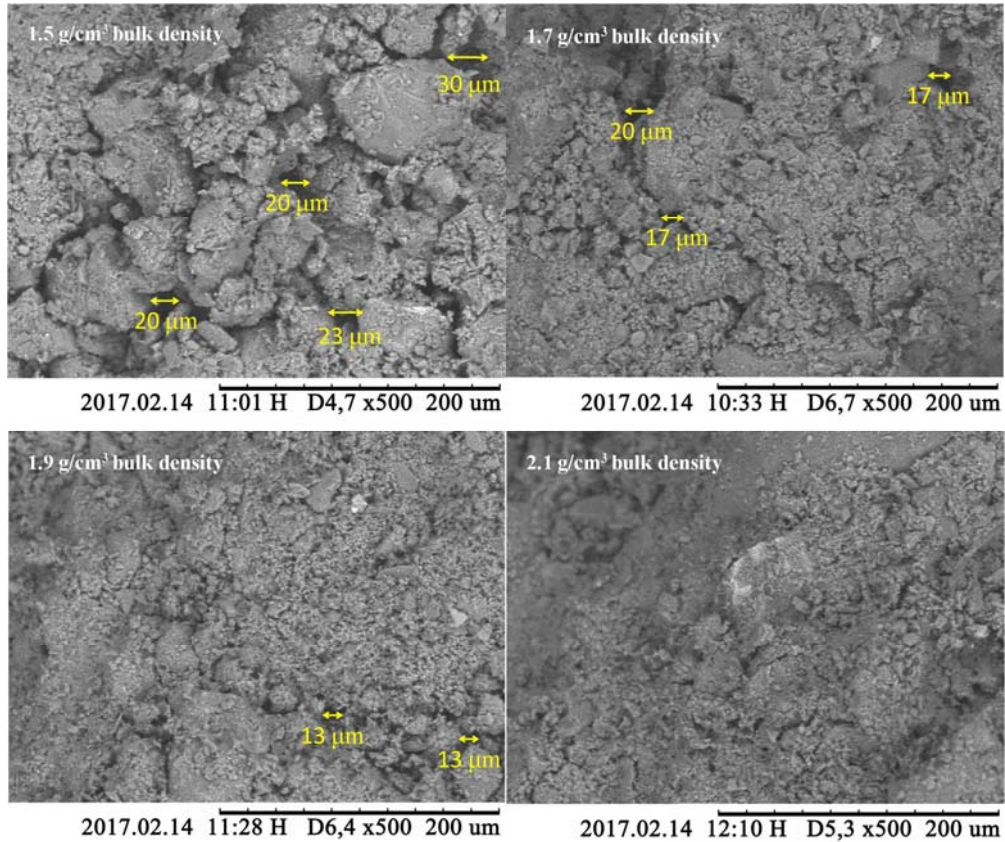
161 TriStar 3000 surface area and porosity analyzer was used to characterize the specific surface area and  
162 pore structure of the samples. The specific surface area, total volume of pores and pore size distribution  
163 are crucial parameters to describe the pore structure of compressed earthen materials. Specific surface  
164 area, pore volume and monolayer adsorption were determined by Brunauer-Emmett-Teller (BET)  
165 method. All the samples were degassed at 250 °C overnight prior the nitrogen adsorption measurements.  
166 The nitrogen adsorption measurements were carried out at -196 °C. The pore size distribution was  
167 determined according to the desorption curve of isotherms using the Barrett-Joiner-Halenda (BJH)  
168 method [29].

### 169 3. Results and discussions

#### 170 3.1. Microstructure of compressed earthen bricks

171 The microstructure images of compressed earthen samples for different bulk densities are illustrated  
172 by scanning electron microscopy (SEM) in Fig. 5. It can be seen that there is a variation of pore quantity  
173 in compressed earthen samples at different bulk densities, the quantity of pore inside the matrix decreases  
174 with increasing bulk density. When the bulk density increases from 1.5 g/cm<sup>3</sup> to 2.1 g/cm<sup>3</sup>, the matrix of

175 compressed earthen bricks becomes more and more compact and the pore diameter reduces significantly.  
176 When the bulk density is  $2.1 \text{ g/cm}^3$ , the visible pores barely exist in matrix of compressed earthen sample,  
177 which leads to a high compactness and a low porosity inside the matrix.

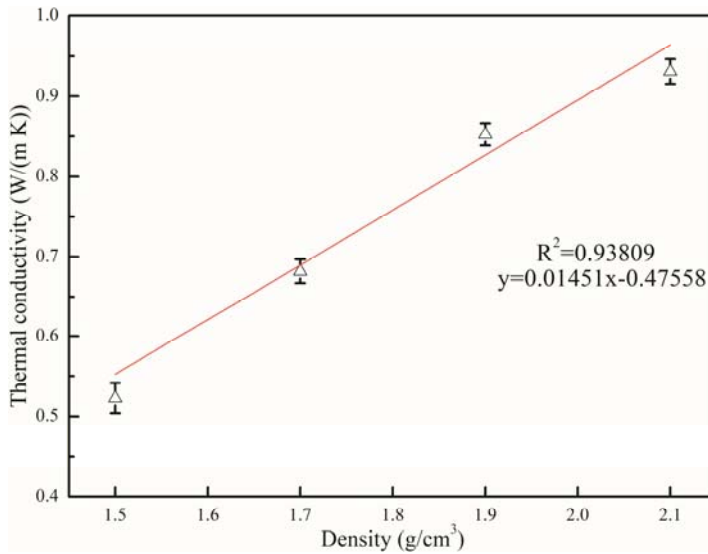


178  
179 Fig. 5 SEM images of compressed earthen materials at different bulk densities.

### 180 3.2. Thermal conductivity

181 Thermal conductivity is one of the crucial parameters which are used to evaluate the thermal insulation  
182 of building materials. The lower thermal conductivity, the lower heat transfer through the building  
183 envelope. The effect of bulk density on thermal conductivity of compressed earthen bricks is presented  
184 in Fig. 6. In detail, the mean values of the thermal conductivity are reported with the uncertainty  
185 calculated as the standard deviation of the mean. As shown in Fig. 6, there is a linear correlation between  
186 the thermal conductivity and the bulk density, where the mean values of the thermal conductivity increase

187 from 0.5228 to 0.9308 W/(m K) with increasing bulk density. This phenomenon can be explained by the  
188 difference of thermal conductivity between air (about 0.026 W/(m K)) and compressed earthen bricks  
189 (between 0.5228 and 0.9308 W/(m K)), and increasing the bulk density will increase the solid content  
190 and decrease the porosity at the same time . In general, the compressed earthen material with low bulk  
191 density has more pores which were filled with air at dry state and the thermal conductivity value of air  
192 is considerably lower than solid phase. Therefore, the compressed earthen material with lower bulk  
193 density has lower thermal conductivity than materials with higher bulk density. The results are similar as  
194 the conclusion in the studies of Tang et al. [15] and Taallah et al. [16].



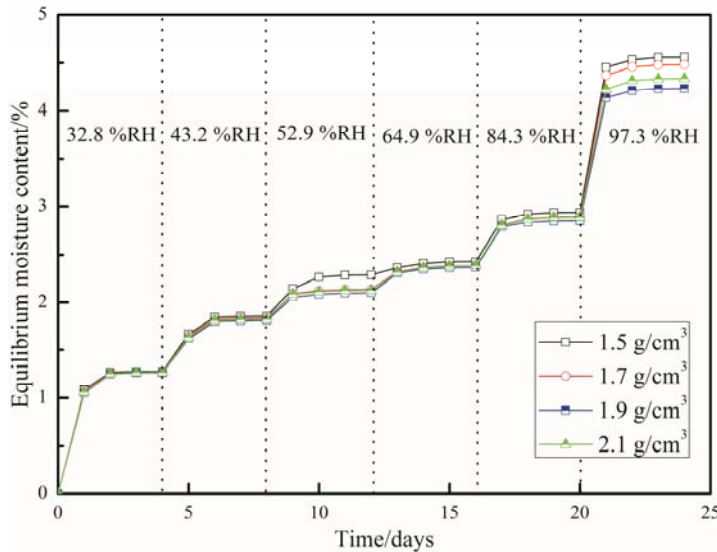
195  
196 Fig. 6 Thermal conductivity vs. bulk density of compressed earthen material.

### 197 3.3. Adsorption-desorption isotherms

198 Fig. 7 shows the evolution of equilibrium moisture content of compressed earthen bricks with different  
199 bulk densities in increasing relative humidity. The evolution with time for compressed earthen bricks  
200 subjected to increasing relative humidity demonstrates that the response of samples to a relative humidity  
201 change is rather fast and equilibrium moisture content values of examples at different bulk densities  
202 usually reach a stabilization in four days. This shows that compressed earthen bricks with different bulk

203 densities can absorb moisture from surrounding with increasing relative humidity to regulate the indoor  
204 relative humidity.

205 It is possible to interpret the impact of bulk density on equilibrium moisture content presented in Fig.  
206 7 by comparing the results of compressed earthen bricks with different bulk densities. It is interesting to  
207 observe that a small variations between the samples existed in the region of high relative humidity.  
208 Further, the equilibrium moisture content at high relative humidity reduces firstly for increasing densities  
209 (from 1.5 g/cm<sup>3</sup> to 1.9 g/cm<sup>3</sup>) and then increases as the bulk density increases from 1.9 g/cm<sup>3</sup> to 2.1 g/cm<sup>3</sup>.  
210 This result indicates that the variation in bulk density slightly impacts the pore structure inside the matrix  
211 as the adsorption at high relative humidity is governed by capillary condensation which is influenced by  
212 the pore structure and pore size inside the matrix.



213  
214 Fig. 7 Evolution of equilibrium moisture content with increasing relative humidity.

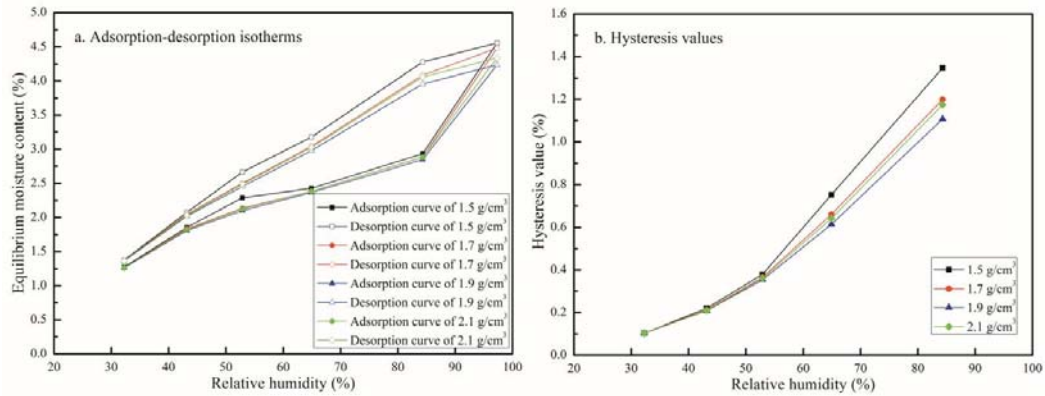
215 Fig. 8 shows the adsorption-desorption isotherms (Fig. 8a) and hysteresis values (Fig. 8b) of  
216 compressed earthen samples at different bulk densities. It can be seen from the adsorption curve,  
217 equilibrium moisture content increases with increasing relative humidity. This phenomenon indicates  
218 that the compressed earthen samples adsorb water vapour from surrounding as relative humidity

219 increases. Two mechanisms are suitable for interpretation of the adsorption [19]: (1) At low relative  
220 humidity, water molecules reach to the pore walls and form a monolayer water film by Van der Waals'  
221 force. (2) As the relative humidity increases, the water film becomes thicker until the narrow pores are  
222 blocked and then the capillary condensation phenomenon occurs. When relative humidity rises and  
223 reaches  $52.89 \pm 0.2$  % RH, the first inflection point is appeared on the adsorption curve. It means the  
224 single layer surface adsorption occurs at the relative humidity of less than  $52.89 \pm 0.2$  % RH and when  
225 relative humidity exceeds  $52.89 \pm 0.2$  % RH, the multilayer surface adsorption occurs. The relative  
226 humidity of  $84.34 \pm 0.1$  % RH is the second inflection point which means the capillary condensation  
227 occurs in narrow pores as relative humidity exceeds  $84.34 \pm 0.1$  % RH.

228 Fgaier et al. [30] presented that the variation in the adsorption behaviour is mainly related to the type  
229 of clay and to the specific surface area of the raw materials. In this study, the adsorption curves of  
230 compressed earthen bricks with different bulk densities are very close to each other. On the one hand,  
231 the samples used in this study have the similar mineral composition as the rural materials were selected  
232 from the same location; on the other hand, it may be explained by the similar specific surface area for  
233 compressed earthen bricks with different bulk densities.

234 Additionally, a distinct difference, which is defined as hysteresis, can be observed between adsorption  
235 and desorption curves as shown in Fig. 8a. McGregor et al. [11] indicated that hysteresis is associated  
236 with capillary condensation caused by micropores and mesopores inside the matrix and it can be used to  
237 evaluate the moisture buffering as an important parameter. As shown in Fig. 8b, the hysteresis values of  
238 compressed earthen bricks increase with increasing relative humidity as the same as Cagnon et al.'s  
239 results [12]. This phenomenon can be explained that when the samples, which have completed the  
240 adsorption process, start to release water vapour to surrounding, the narrow pores are blocked with

241 condensed water leads to the adsorbed water molecules can't evaporate outward and then hysteresis  
 242 occurs. With relative humidity reduces to the degree corresponding to Kelvin's radius, capillary  
 243 evaporation releases condensed water to surrounding in favour of developing a desorption process and  
 244 then the hysteresis value reduces with decreasing relative humidity. Fig. 8b also shows that the hysteresis  
 245 value increases firstly and then decreases with increasing bulk density at a given relative humidity. This  
 246 result can be interpreted by compactness variation caused by change of bulk density. Fgaier et al. [30]  
 247 presented a loose soil matrix that had an open texture which facilitated the entry and release of water  
 248 vapour and impeded increasing of the hysteresis value. When the bulk density increases to  $2.1 \text{ g/cm}^3$ ,  
 249 increasing of hysteresis values may be explained by increasing amount of mesopores as capillary  
 250 condensation, which is the reason for hysteresis, usually appears in mesopores [11].



251  
 252 Fig. 3 Adsorption-desorption isotherms and hysteresis values of compressed earthen samples at different bulk densities

### 253 3.4. Porosity

254 Nitrogen adsorption-desorption isotherms of compressed earthen bricks with different bulk densities  
 255 are examined in order to characterise the effect of porosity on the hygroscopic behaviour. Nitrogen  
 256 adsorption-desorption isotherms results are presented in Table 3 in terms of specific surface area and  
 257 pore volume calculated by the BET method, and average pore width obtained with the BJH method.

258 Table 3 Results of porous structure.

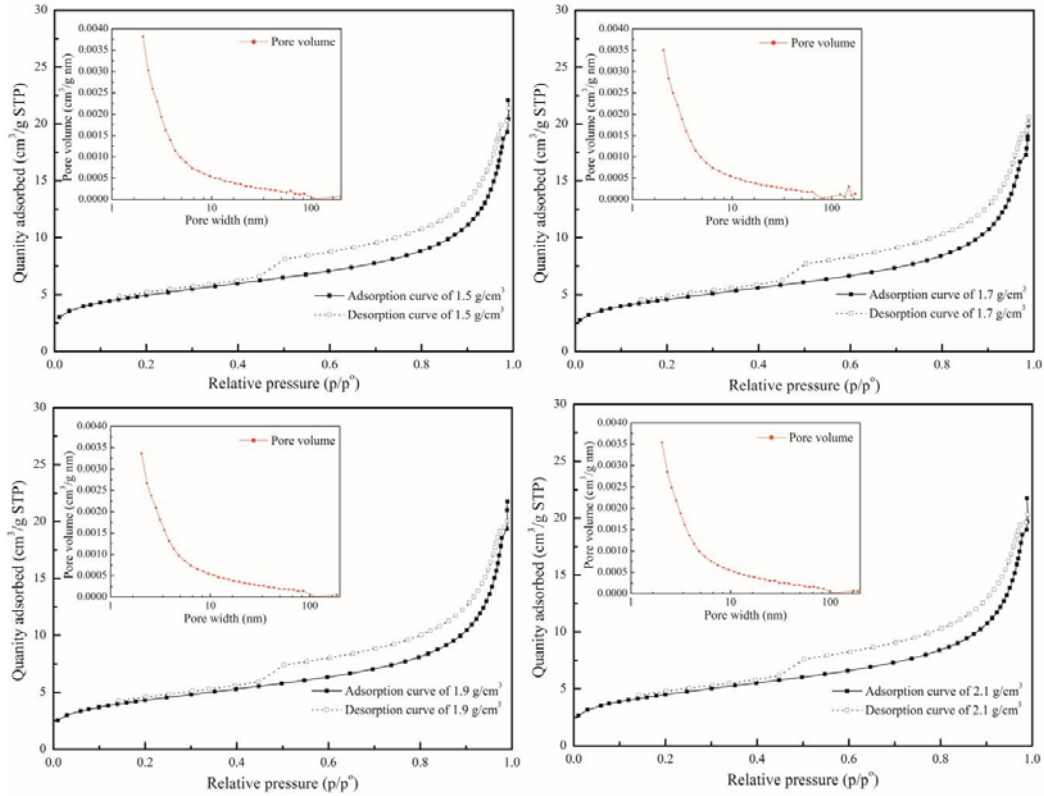
| Bulk density<br>(g/cm <sup>3</sup> ) | Specific surface area (m <sup>2</sup> /g) | Micropore volume (cm <sup>3</sup> /g) | Mesopore volume (cm <sup>3</sup> /g) | Average pore width (nm) |
|--------------------------------------|---|---------------------------------------|--------------------------------------|-------------------------|
| 1.50                                 | 17.7023                                   | 0.001221                              | 0.032239                             | 8.2406                  |
| 1.70                                 | 16.4277                                   | 0.001118                              | 0.031268                             | 8.2988                  |
| 1.90                                 | 15.5008                                   | 0.000867                              | 0.030785                             | 8.3446                  |
| 2.10                                 | 16.2091                                   | 0.000937                              | 0.031019                             | 8.1649                  |

259 Specific surface area is a key indicator to evaluate the adsorption capacity of porous materials. Fgaier  
 260 et al. [30] demonstrated a series of experiments for three types of unfired clay bricks and the results  
 261 showed that the bricks with higher specific surface area have higher adsorption capacity. The  
 262 experimental values are distributed between 15 and 18 m<sup>2</sup>/g in this study, compared with 1 to 4 m<sup>2</sup>/g in  
 263 Raimondo et al.'s study [22] and 4 to 15 m<sup>2</sup>/g in Arrigoni et al.'s study [31]. These results interpret that  
 264 compressed earthen bricks in this study have a larger adsorption capability (between 2.30 % and 2.50 %  
 265 at 64.92 %RH) than the existing studies (the highest value in Arrigoni et al.'s study is 2.028 % at 58 %RH).  
 266 Then, a slight difference in the specific surface area between compressed earthen bricks with different  
 267 bulk densities leads to the tested samples have a similar adsorption behaviour as shown in Fig. 7. In  
 268 addition, the tiny differences in the equilibrium moisture content between compressed earthen bricks  
 269 with different bulk densities at high relative humidity are caused by the slight differences in mesopore  
 270 volume of samples. The micropore volume reveals the hygroscopic ability at low relative humidity and  
 271 the mesopore volume are responsible for capillary condensation and hysteresis [9]. Furthermore, the  
 272 relationship between mesopore volume and bulk density results in the hysteresis value firstly reduces  
 273 and then increases with increasing bulk density.

274 Nitrogen adsorption-desorption isotherms and BJH desorption pore volume curves of compressed  
 275 earthen samples at different bulk densities are shown in Fig. 9. Adsorption-desorption isotherms at  
 276 different bulk densities express the same trend with relative pressure changes and the distinct hysteresis

277 loops existed between adsorption and desorption isotherms. According to a classification of  
278 physisorption isotherms raised by the IUPAC in 1984, the hysteresis loops in this study are associated  
279 with capillary condensation taking place in mesopores which are between 2 to 50 nm in diameter [29].  
280 The IUPAC classified hysteresis loops in 4 types and related them with pore structures [32]. The  
281 hysteresis loops in this study belong to the type H3 hysteresis loops which is observed with aggregates  
282 of platelike particles. Isotherms with type H3 hysteresis loops indicate that the pores existed in the  
283 examples may include micropores or mesopores which interconnect to form a slitlike pore [33]. The  
284 compressed earthen bricks in this study contain amounts of clay minerals which demonstrate a platy  
285 structure and there are many slitlike pores in the matrix of samples as shown in Fig. 5. In addition, the  
286 absorption curves at different bulk densities are biased toward vertical coordinates when the relative  
287 pressure of nitrogen is less than 0.1 and absorbed quantity values are lower than  $5 \text{ cm}^3/\text{g}$ , showing that  
288 the existing micropore volume values in the samples are very small. Then, the absorption curves rapidly  
289 raise in the high relative pressure phase, demonstrating the existing pores in the samples may be  
290 composed of irregular pores which are formed by accumulation of earthen materials.





291

292 Fig. 4 Nitrogen adsorption-desorption isotherms and BJH desorption pore volume results.

293 According to the existence of hysteresis between adsorption and desorption  
 294 isotherms curves were used to analyze the distribution of the mesopores' widths. As shown in Fig. 9,  
 295 there is no obvious peak in the BJH desorption pore volume curves of compressed earthen samples at  
 296 different bulk densities. It reveals that the pore size of compressed earthen materials distributes in a high  
 297 content and that no uniform pore structure exist in compressed earthen samples.

## 298 4. Conclusions

299 This study presented a series of experimental analyses for the thermal conductivity and hygroscopic  
 300 behaviour of compressed earthen bricks at different bulk densities. The effect of bulk density on  
 301 hygrothermal properties may be summarized as follows:

302 1. The thermal conductivity of compressed earthen bricks linearly increased with increasing bulk

303 density. This phenomenon might be explained by both porosity and pore diameter inside the matrix  
304 decreased with increasing bulk density.

305 2. The moisture content in compressed earthen bricks with different bulk densities reached an  
306 equilibrium within four days after the relative humidity changed, which indicated that compressed  
307 earthen bricks can be used to regulate the indoor relative humidity.

308 3. Compressed earthen bricks adsorbed water vapour from surrounding as relative humidity increased  
309 according to single layer surface adsorption, multilayer surface adsorption and capillary condensation.

310 4. Compressed earthen bricks in this study have a larger adsorption capability to stabilize indoor  
311 relative humidity than in earlier studies.

312 5. There are many slitlike pores in the matrix of samples and the pore size of compressed earthen  
313 materials distributes in a high content.

## 314 Acknowledgements

315 This study is supported by The National Science Fund for Distinguished Young Scholars in China  
316 (Project No. 51325803). Lei Zhang thanks the financial support from China Scholarship Council and  
317 Research Council of Norway (Project No. 263919). The authors thank also The Research Centre on  
318 Zero Emission Neighbourhoods in Smart Cities (ZEN) and NanoLab at NTNU for the support in  
319 carrying out the experiments. The Research Council of Norway is acknowledged for the support to the  
320 Norwegian Micro- and Nano-Fabrication Facility, NorFab.

## 321 References

322 [1] IEA 2015. Energy and climate change.

323 <https://www.iea.org/publications/freepublications/publication/WEO2015SpecialReportonEnergyandClimateChange.pdf>

- 324 [2] X.W. Liu, Y.M. Chen, H. Ge, P. Fazio, G.J. Chen, X.G. Guo. Determination of optimum insulation thickness for building  
325 walls with moisture transfer in hot summer and cold winter zone of China. *Energy Build* 2015; 109: 361-8.
- 326 [3] D.B. Özkan, C. Onan. Optimization of insulation thickness for different glazing areas in buildings for various climatic regions  
327 in Turkey. *Appl energy* 2011; 88: 1331-42.
- 328 [4] A.G. Hestnes, N.L. Eik-Nes. *Zero Emission Building*. Project report 2016. Trondheim: NTNU.
- 329 [5] L. Soudani, A. Fabbri, J.C. Morel, M. Woloszyn, P.A. Chabriac, H. Wong, A.C. Grillet. Assessment of the validity of some  
330 common assumptions in hygrothermal modeling of earth based materials. *Energy Build* 2016; 116: 498-511.6]
- 331 [6] X. Dong, V. Soebarto, M. Griffith. Achieving thermal comfort in naturally ventilated rammed earth houses. *Build Environ*  
332 2014; 82: 588-598.
- 333 [7] M. Hall, D. Allinson. Analysis of the hygrothermal functional properties of stabilised rammed earth materials. *Build Environ*  
334 2009; 44: 1935-42.
- 335 [8] M. Ozel. Determination of optimum insulation thickness based on cooling transmission load for building walls in a hot  
336 climate. *Energy Convers Manag* 2013; 66: 106-14.
- 337 [9] S. Liuzzi, M.R. Hall, P. Stefanizzi, S.P. Casey. Hygrothermal behaviour and relative humidity buffering of unfired and  
338 hydrated lime-stabilised clay composites in a Mediterranean climate. *Build Environ* 2013; 61: 82-92.
- 339 [10] Q.D. Li, R.Y. You, C. Chen, X.D. Yang. A field investigation and comparative study of indoor environmental quality in  
340 heritage Chinese rural buildings with thick rammed earth wall. *Energy Build* 2013; 62: 286-83.
- 341 [11] F. McGregor, A. Heath, E. Fodde, A. Shea. Conditions affecting the moisture buffering measurement performed on  
342 compressed earth blocks. *Build Environ* 2014; 75: 11-8.
- 343 [12] H. Cagnon, J.E. Aubert, M. Coutand, C. Magniont. Hygrothermal properties of earth bricks. *Energy Build* 2014; 80: 208-17.
- 344 [13] M. Hall, D. Allinson. Assessing the effects of soil grading on the moisture content-dependent thermal conductivity of  
345 stabilised rammed earth materials. *Appl Therm Eng* 2009; 29: 740-7.

- 346 [14] M.B. Mansour, A. Jelidi, A.S. Cherif, S.B. Jabrallah. Optimizing thermal and mechanical performance of compressed earth  
347 blocks (CEB). *Constr Build Mater* 2016; 104: 44-51.
- 348 [15] A.M. Tang, Y.J. Cui, T.T. Le. A study on the thermal conductivity of compacted bentonites. *Appl Clay Sci* 2008; 41: 181-9.
- 349 [16] B. Taallah, A. Guettala. The mechanical and physical properties of compressed earth block stabilized with lime and filled  
350 with untreated and alkali-treated date palm fibers. *Constr Build Mater* 2016; 104: 52-62.
- 351 [17] T. Ashour, A. Korjenic, S. Korjenic, W. Wu. Thermal conductivity of unfired earth bricks reinforced by agricultural wastes  
352 with cement and gypsum. *Energy Build* 2015; 104: 139-46.
- 353 [18] E.A. Adam, P.J. Jones. Thermophysical properties of stabilised soil building blocks. *Build Environ* 1995; 30: 245-53.
- 354 [19] T. Ashour, H. Georg, W. Wu. An experimental investigation on equilibrium moisture content of earth plaster with natural  
355 reinforcement fibres for straw bale buildings. *Appl Therm Eng* 2011; 31: 293-303.
- 356 [20] T. Ashour, A. Korjenic, S. Korjenic. Equilibrium moisture content of earth bricks biocomposites stabilized with cement and  
357 gypsum. *Cem Concr Compos* 2015; 59: 18-25.
- 358 [21] F. McGregor, A. Heath, A. Shea, M. Lawrence. The moisture buffering capacity of unfired clay masonry. *Build Environ*  
359 2014; 82: 599-607.
- 360 [22] M. Raimondo, M. Dondi, F. Mazzanti, P. Stefanizzi, P. Bondi. Equilibrium moisture content of clay bricks: The influence of  
361 the porous structure. *Build Environ* 2007; 42: 926-932.
- 362 [23] L. Randazzo, G. Montana, A. Hein, A. Castiglia, G. Rodonò, D.I. Donato. Moisture absorption, thermal conductivity and  
363 noise mitigation of clay based plasters: The influence of mineralogical and textural characteristics. *Appl Clay Sci* 2016; 132-  
364 133: 498-507.
- 365 [24] Standardization Administration of the People's Republic of China. GB/T 50123-1999. Standard for soil test method. Beijing:  
366 Standards Press of China; 1999.(in Chinese)
- 367 [25] Ministry of Transport of the People's Republic of China. JTJ 051-93. Test methods of soils for highway engineering.

368 Beijing: China Communications Press; 1993.(in Chinese)

369 [26] H.Y. Yu, L. Zheng, J.J. Yang, L.L. Yang. Stabilised compressed earth bricks made with coastal solonchak. Constr Build

370 Mater 2015; 77: 409-18.

371 [27] Standardization Administration of the People's Republic of China. GB/T 20312-2006. Hygrothermal performance of

372 building materials and products-Determination of hygroscopic sorption properties. Beijing: Standards Press of China;

373 2006.(in Chinese)

374 [28] ISO/DIS 22007-2, Plastics - Determination of thermal conductivity and thermal diffusivity - Part 2: Transient plane source

375 method.

376 [29] F. Collet, M. Bart, L. Serres, J. Miriel. Porous structure and water vapour sorption of hemp-based materials. Constr Build

377 Mater 2008; 22: 1271-80.

378 [30] F.E. Fgaier, Z. Lafhaj, C. Chapiseau, E. Antezak. Effect of sorption capacity on thermo-mechanical properties of unfired

379 clay bricks. J Build Eng 2016; 6: 86-92.

380 [31] A. Arrigoni, A.C. Grillet, R. Pelosato, G. Dotelli, C.T.S. Beckett, M. Woloszyn, D. Ciancio. Reduction of rammed earth's

381 hygroscopic performance under stabilisation: an experimental investigation. Build Environ 2017; 115: 358-67.

382 [32] K.S.W. Sing, R.T. Williams. Physisorption hysteresis loops and the characterization of nanoporous materials. Adsorpt Sci

383 Technol 2004; 22: 773-82.

384 [33] M. Kruk, M. Jaroniec. Gas adsorption characterization of ordered organic-inorganic nanocomposite materials. Chem Mater

385 2001; 13: 3169-83.